Research paper

Study on the subgrade service depth of moving vehicles under multi-wheeled superposition effect

Yanmin Zhou[1], Haiyang Wang[2], Lingyun Kong[3], Jialiang Liu[4], Jie Wang[5], Zhimei Wang[6]

Abstract: The stress superposition effect in the midline area of the multi-wheeled vehicles produced by moving vehicles load is generally ignored, which leads to smaller results in research of subgrade service depth. Based on the elastic mechanics theory, the analytical solution of subgrade dynamic response under moving vehicles load is derived with compound elastic layers. The characteristics of subgrade dynamic stress distribution under the action of moving vehicles are analyzed by using Midas Gts Nx numerical simulation software, and the influence of static and dynamic axle load on the subgrade service depth is compared. The results demonstrate that the subgrade dynamic stress in the under-wheel area attenuates rapidly along the depth direction, while the subgrade dynamic stress in the midline area increases at first and subsequently decreases along the same direction. With the increase of subgrade dynamic stress, the shape of dynamic stress isosurface changes from bimodal to unimodal. Whether in the form of static or dynamic axle load, the subgrade service depth in the middle line area is larger than that in under-wheel area, and the influence of dynamic axle load on the subgrade service depth is greater than that of static axle load. The wheel distance and vehicle velocity have a significant influence on the subgrade service depth. With the increase of vehicle velocity, the subgrade service depth decreases. With the increase of wheel distance, the subgrade service depth decreases.

Keywords: road engineering, moving vehicles, superposition effect, numerical simulation, subgrade service depth

[1]M.Sc., Eng., School of Civil Engineering, Chongqing Jiaotong University, Chongqing 400074, China, e-mail: zhouyanmincqjtu@163.com, ORCID: 0000-0002-1213-7165

[2]Associate Prof., PhD., Eng., School of Civil Engineering, Chongqing Jiaotong University, Chongqing 400074, China, e-mail: wanghaiyang_cq@cqjtu.edu.cn, ORCID: 0000-0002-7152-5969

[3]Prof., PhD., Eng., School of Civil Engineering, Chongqing Jiaotong University, Chongqing 400074, China, e-mail: klyyqr2002@163.com, ORCID: 0000-0003-3886-8254

[4]Associate Prof., PhD., Eng., School of Civil Engineering, Chongqing Jiaotong University, Chongqing 400074, China, e-mail: 287500275@qq.com, ORCID: 0000-0002-4463-2312

[5]M.Sc., Eng., School of Civil Engineering, Chongqing Jiaotong University, Chongqing 400074, China, e-mail: gcwangjie@163.com, ORCID: 0000-0003-3270-4216

[6]M.Sc., Eng., School of Civil Engineering, Chongqing Jiaotong University, Chongqing 400074, China, e-mail: 14372241@qq.com, ORCID: 0000-0001-6859-3795

1. Introduction

Nowadays, the whole world is advocating the construction of conservation-oriented highways. Reducing the height of subgrade could not only reduce the cost of highway construction, but also reduce the use of land resources. The main body of road structure is divided into pavement, subgrade and soil foundation, and the settlement of roads mostly comes from subgrade settlement. The reduction of highway subgrade height means that the subgrade service depth will change. Once the subgrade service depth under vehicle load action invades the soil foundation, it will lead to greater road settlement. Traffic load has a great influence on subgrade settlement of highways [1]. Shanghai, China, Metro Line 1 hardly caused settlement in more than two years after it was completed and before it was opened to traffic, but the settlement reached 30–60 mm in eight months after it was opened to traffic and 140 mm within four years, the current calculation method of subgrade service depth in most area of the world is based on the elastic half-space theory under static load, the wheel load is assumed to be static load, and Boussinesq solution is used to determine the subgrade service depth under vehicle action. The Boussinesq solution is mainly aimed at the elastic semi-infinite space, and the diffusion of load can not be taken into account, but the road is a layered structure, so it will produce large errors [1, 2]. In fact, the traffic load acting on road surface is a kind of dynamic load whose size and position change at all times, and the contact between tire and ground belongs to surface source contact. Momoya [3] et al. simulated the long-term deformation development law of subgrade under the action of single-wheel fixed-point loading and moving loading through 1:5 laboratory model test. The results show that moving vehicle load will lead to greater permanent deformation of subgrade. Therefore, the influence of moving vehicle load on subgrade deformation cannot be ignored, and the studying of the subgrade service depth of road under moving vehicle load is an important basis for calculating road settlement [4].

Research on analytical solution of composite layered road structure under the action of moving loads: Liu Dapeng [2] studied the influence of subgrade moisture content and subgrade height on subgrade service depth through field measurement and similar model test. Lu Zheng [4] et al. believe that under the traffic load, the deformation of the road structure is mainly elastic deformation, and they use the theory of elasticity to derive the analytical solution of the mechanical response of the composite elastic layer under the action of moving vehicles. The effects of subgrade elastic modulus and overloading on the subgrade service depth are analyzed. The analytical solution of the mechanical response of the composite elastic layer under moving load is derived by using the theory of elasticity combined with the integral transformation method, and compared with the finite element results, it is proved that the analytical solution of elasticity has sufficient accuracy [4–6]. In addition, Liu [7] and Fang [8] studied the dynamic stress distribution of subgrade under train moving load by numerical simulation. It is found that when the two vibration sources are close, the dynamic stress distribution of subgrade shows a strong superposition phenomenon.

At present, in the research of subgrade influence depth under the action of moving vehicle load, the under-wheel area is usually assumed to be the area most affected by

the action of vehicle load [9–14] which ignores the stress superposition effect produced by vehicles in the process of passing, or the calculations are made using static force according to the specification, resulting in relatively smaller calculated values of subgrade service depth. In view of the above issues, formula derivation on the dynamic mechanical response of composite elastic layer under the action of moving vehicle load is carried out in this paper by combining elasticity and integral transform method. Furthermore, through the numerical simulation of the road model under the action of moving vehicle load, the distribution characteristics of dynamic stress and the influencing factors of subgrade service depth are studied.

2. Dynamic response analytical solution under the action of moving vehicle load

2.1. Calculation model of composite elastic layer structure under moving vehicle load action

The road structure is subjected to low amplitude and multi-cycle vehicle load on a long-term basis. The deformation of the road structure under the action of a single-time moving vehicle load is dominated by elastic deformation. This paper assumes that the layered system of road is elastic layered medium, which can meet the precision requirements of practical engineering applications. When a vehicle runs normally, the tires move in uniform circular motion, and its loading mode is rolling loading. Assuming that the moving vehicle load is a rectangular load distributed vertically and uniformly, and the vehicle load is expressed by cosine function, the moving vehicle load is defined as Formulas (2.1)–(2.2). Fig. 1 is a calculation model of composite elastic layer structure under moving vehicle load action. Where, E_i is the resilience modulus of the i-th layer structure, h_i is the thickness of the i-th layer structure, ρ_i is the density of the i-th layer structure, μ_i is the Poisson's ratio of
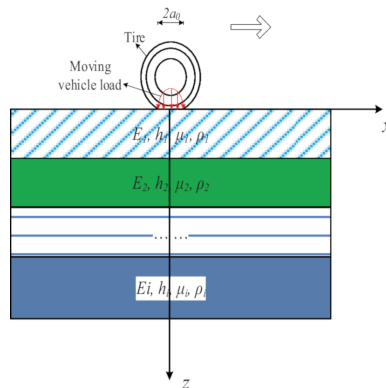

Fig. 1. Calculation model of moving vehicle with composite elastic layers

the i-th layer structure, V s the moving speed of the vehicle load, the touchdown shape of the moving vehicle load is rectangular, and the side length parallel to the forward direction is $2a_0$.

$$(2.1) \qquad \sigma_z(x,0) = \begin{cases} P_z \cos\left(\dfrac{\pi x}{2a_0}\right), & |x - Vt| \le a_0 \\ 0, & |x - Vt| \ge a_0 \end{cases}$$

$$(2.2) \qquad \tau_{zx}(x,0) = \begin{cases} 0, & |x - Vt| \le a_0 \\ 0, & |x - Vt| \ge a_0 \end{cases}$$

where $\sigma_z(x,0)$ is vertical dynamic stress in plane subgrade soil at $z = 0$. $\tau_{zx}(x,0)$ is horizontal dynamic stress in plane subgrade soil at $z = 0$. P_z is peak value of impact load. t is time.

By jointly solving the geometric equation, physical equation and motion equation in elasticity, the Lame equation [5], [6] as shown in equation (2.3) is obtained:

$$(2.3) \qquad \begin{cases} G\left(\dfrac{\partial^2}{\partial x^2} + \dfrac{\partial^2}{\partial z^2}\right)u + (\lambda + G)\dfrac{\partial}{\partial x}\left(\dfrac{\partial u}{\partial x} + \dfrac{\partial w}{\partial z}\right) = \rho\dfrac{\partial^2 u}{\partial t^2} \\ G\left(\dfrac{\partial^2}{\partial x^2} + \dfrac{\partial^2}{\partial z^2}\right)w + (\lambda + G)\dfrac{\partial}{\partial z}\left(\dfrac{\partial u}{\partial x} + \dfrac{\partial w}{\partial z}\right) = \rho\dfrac{\partial^2 w}{\partial t^2} \end{cases}$$

where u and w are Displacements in x-direction and z-direction, respectively, ρ is Soil density. λ and G are Lame constant, $\lambda = \dfrac{\mu E}{(1 + \mu)(1 - 2\mu)}$, $G = \dfrac{E}{2(1 + \mu)}$.

2.2. Galilean and Fourier transforms

Clearly, coordinate x is related to vehicle speed V and time t, that is, so there exists a Galilean transform as shown in Formula (2.4):

$$(2.4) \qquad x' = x - Vt$$

Carry out Fourier transform for x-direction displacement $u(x', z)$, z-direction displacement $w(x', z)$ and moving cosine vehicle load, and we can get Formulas (2.5)–(2.7):

$$(2.5) \qquad \begin{cases} \overline{u}(\xi_1, z) = \displaystyle\int_{-\infty}^{+\infty} u(x', z)e^{-i\xi_1 x'}\,\mathrm{d}x' \\ \overline{w}(\xi_1, z) = \displaystyle\int_{-\infty}^{+\infty} w(x', z)e^{-i\xi_1 x'}\,\mathrm{d}x' \end{cases}$$

$$(2.6) \qquad \sigma_z(\xi_1, 0) = \begin{cases} \dfrac{P_z \pi \cos(\xi_1 a_0)}{a_0\left[\left(\dfrac{\pi}{2a_0}\right)^2 - \xi_1^2\right]}, & |\xi_1| \le a_0 \\ 0, & |\xi_1| \ge a_0 \end{cases}$$

$$(2.7) \qquad \tau_{zx}(\xi_1, 0) = \begin{cases} 0, & |\xi_1| \leq a_0 \\ 0, & |\xi_1| \geq a_0 \end{cases}$$

where, $\overline{u}$ and $\overline{w}$ are Fourier transforms of u and w to x' coordinates. ξ_1 is frequency domain coordinate of coordinate x after Galilean transform and Fourier transform.

2.3. Dynamic response analytical solution of composite elastic layer

Formula (2.8) can be obtained from geometric equation, physical equation and motion equation in elasticity:

$$(2.8) \qquad \frac{\partial}{\partial z} \begin{bmatrix} \overline{u} & \overline{w} & \tau_{zx} & \sigma_z \end{bmatrix}^T = A \begin{bmatrix} \overline{u} & \overline{w} & \tau_{zx} & \sigma_z \end{bmatrix}^T$$

Based on modern control theory[6], the solution of Formula (2.9) is:

$$(2.9) \qquad \begin{bmatrix} \overline{u}(\xi_1, z) \\ \overline{w}(\xi_1, z) \\ \overline{\tau}_{zx}(\xi_1, z) \\ \overline{\sigma}_z(\xi_1, z) \end{bmatrix} = T \begin{bmatrix} \overline{u}(\xi_1, 0) \\ \overline{w}(\xi_1, 0) \\ \overline{\tau}_{zx}(\xi_1, 0) \\ \overline{\sigma}_z(\xi_1, 0) \end{bmatrix},$$

where, T is the transfer matrix, which transfers the surface stress-strain matrix to an arbitrary depth, that is, establishes the relationship between the boundary condition of $z = 0$ surface and the mechanical response at an arbitrary depth. The matrix T is the matrix power of an exponent. Furthermore, according to the matrix theory, the solution method of the transfer matrix T is obtained as Formula (2.10):

$$(2.10) \qquad T = e^{Az} = P e^{\text{diag}(b, a, -b, -a)z} P^{-1}$$

where $\pm a$ and $\pm b$ are eigenvalues of matrix A, $a^2 = \left(1 - \dfrac{V^2}{v_s^2}\right)\xi_1^2$ and $b^2 = \left(1 - \dfrac{V^2}{v_p^2}\right)\xi_1^2$, v_p is longitudinal wave velocity, v_s is transverse wave velocity, and $v_P^2 = \dfrac{\lambda + 2G}{\rho} v_s^2 = \dfrac{G}{\rho}$. P is eigenvector matrix of matrix A.

From this, the formula for mechanical response at an arbitrary depth z can be obtained, as shown in Formula (2.11):

$$(2.11) \qquad \begin{bmatrix} \overline{u}(\xi_1, z) \\ \overline{w}(\xi_1, z) \\ \overline{\tau}_{zx}(\xi_1, z) \\ \overline{\sigma}_z(\xi_1, z) \end{bmatrix} = {}^N T \left(\xi_1, z - \sum_{i=1}^{N-1} h_i \right) \prod_{i=1}^{N-1} {}^i T(\xi_1, h_i) \begin{bmatrix} \overline{u}(\xi_1, 0) \\ \overline{w}(\xi_1, 0) \\ \overline{\tau}_{zx}(\xi_1, 0) \\ \overline{\sigma}_z(\xi_1, 0) \end{bmatrix}$$

where N is ordinal number of the current calculation layer, h_i is thickness of the i-th layer structure, ${}^i T$ is transfer matrix of the i-th layer structure.

Furthermore, there exists a boundary condition: when the depth approaches to infinity, its stress and strain converge to 0, then, we can get Formula (2.12):

$$(2.12) \quad \begin{bmatrix} \overline{u}\,(\xi_1,0) \\ \overline{w}\,(\xi_1,0) \end{bmatrix} = - \begin{bmatrix} F_{11} & F_{12} \\ F_{21} & F_{22} \end{bmatrix}^{-1} \begin{bmatrix} F_{13} & F_{14} \\ F_{23} & F_{24} \end{bmatrix} \begin{bmatrix} \overline{\tau}_{zx}\,(\xi_1,0) \\ \overline{\sigma}_z\,(\xi_1,0) \end{bmatrix}$$

where, $F_{4\times4} = {}^nT\left(\xi_1, \infty - \sum\limits_{i=1}^{n-1} h_i\right) \prod\limits_{i=1}^{n-1} {}^iT\,(\xi_1, h_i)$.

Substitute Formula (2.12) back into Formula (2.11), and carry out Galilean and Fourier inverse transform to obtain Formula (2.13):

$$(2.13) \quad R(x, z, t) = \frac{1}{2\pi} \int\limits_{-\infty}^{+\infty} \overline{R}\,(\xi_1, z)\, e^{i\xi_1(x - Vt)}\, \mathrm{d}\xi_1$$

where $\overline{R}\,(\xi_1, z)$ is mechanical response analytical solution of an arbitrary point after Fourier

transform, $\overline{R}\,(\xi_1, z) = \begin{bmatrix} \overline{u}\,(\xi_1, z) \\ \overline{w}\,(\xi_1, z) \\ \overline{\tau}_{zx}\,(\xi_1, z) \\ \overline{\sigma}_z\,(\xi_1, z) \end{bmatrix}$, $R(x, z, t)$ is mechanical response analytical solution

of composite elastic layer system at an arbitrary time and arbitrary point.

3. Dynamic stress superposition characteristics under the action of moving vehicle load

3.1. Numerical simulation scheme design

For a road structure, the mechanical parameters of the surface course, base course and soil foundation are not much different. When calculating the dynamic response of the structure, Odemark Formula (3.1) [15, 16] is often used to convert the thickness of the surface course structure into the equivalent pavement thickness consistent with the resilient modulus of the base course:

$$(3.1) \quad H_e = \left(\frac{E}{E_1}\right)^{1/3} H$$

where H_e is equivalent thickness after conversion, E is resilience modulus before conversion, H is original thickness, E_1 is reference resilience modulus of base course.

Because the distance between the front and rear axles is large and the dynamic response produced by the front axle is small, this paper mainly analyzes the dynamic response produced by the rear axle [17]. To realize the moving loading in the finite element software, firstly, a load moving belt is set in the load moving direction, and the belt is divided into several parts for gradual loading [18]. When the tire touchdown pressure reaches the peak

value in a certain grid unit, the tire just completely enters the grid unit, and at the next unit moment, the tire starts to drive into the next grid unit. Therefore, when the impact load in the previous grid unit reaches the peak value, the next grid unit starts to load, that is, it can simulate the process of the continuous moving loading of a vehicle, and the loading process is shown in Fig. 2.
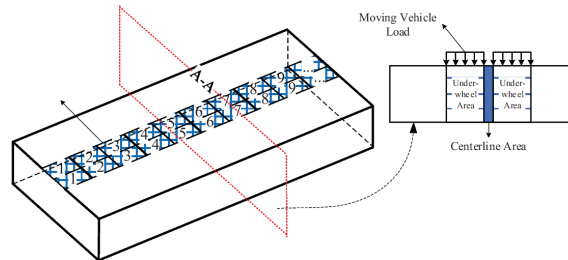

Fig. 2. Load moving belt

When calculating, 100 kN (single-axle double-wheel set) is adopted for axle load, 25 kN for single-wheel load (P) and 0.7 MPa for touchdown pressure (q). The tire touchdown shape is rectangular, and its length and width can be calculated by Formula (3.2):

$$(3.2) \qquad \begin{cases} A_{cb} = \dfrac{P}{q} \\[2mm] K = \sqrt{\dfrac{A_{cb}}{0.5227}} \\[2mm] L = 0.8712K \\[1mm] B = 0.6K \end{cases}$$

where A_{cb} is touchdown area, m^2. K is distribution coefficient. L is long side Length, m. B is Short side length, m.

Considering that the touchdown area increases with the axle load under overload condition, the Empirical Formula (3.3) of axle load P and touchdown area A in Belgian method [4, 16] is adopted:

$$(3.3) \qquad A = 8 \cdot 10^{-7}P + 0.0152$$

Assume that when the vehicle runs normally, the moving vehicle load is a rectangular load with vertical uniform distribution, and the peak value of the vehicle load is expressed by trigonometric function, as shown in Formula (3.4):

$$(3.4) \qquad \begin{cases} P_1 = P_z \sin(\omega_1 t) \\[2mm] \omega_1 = 2\pi \left(\dfrac{V}{2L} \right) \end{cases}$$

where P_1 is impact load, kN/m^2, t is time, s.

In order to compare the difference between the dynamic research method and the static research method, this paper sets the comparative working condition under static loading. The static load distribution is in the form of trigonometric function, as shown in Formula (3.5):

(3.5)
$$
\begin{cases}
P_2 = P_z \sin(\omega_2 y) \\
\omega_2 = 2\pi \left(\dfrac{1}{2L} \right)
\end{cases}
$$

3.2. Verification of numerical simulation scheme

For the correctness of the numerical simulation scheme, the field measured data in reference [5] are used for comparison with the numerical calculation results. The model is consists of four courses, namely, surface course, base course, subgrade and soil foundation from top to bottom, with the thickness of 0.18 m, 0.5 m, 3.2 m and 5 m respectively, and the grade of the subgrade side slope is 1:1.5. Fig. 3 shows a typical three-course road system composed of equivalent pavement, subgrade and semi-infinite foundation. Table 1 shows the parameters of numerical simulation. The viscous boundary conditions are set at four sections, with fixed boundaries set at the bottom.
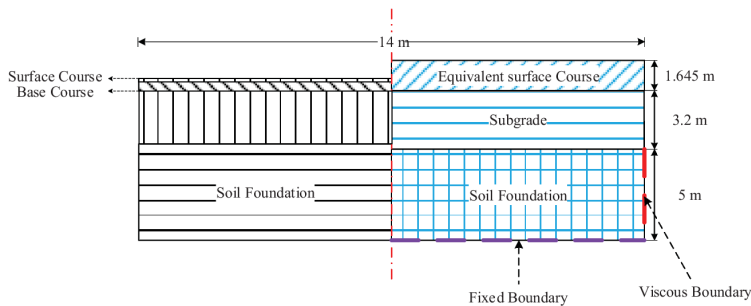

Fig. 3. Onsite model to Calculation model

Table 1. Calculation parameters of each layer material

Courses	Resilient modulus (MPa)	Density (kg/cm^3)	Cohesion (kPa)	Internal friction angle (°)	Poisson's ratio	Damping ratio
Equivalent surface Course	100	2300	–	–	0.25	0.12
Subgrade	100	2000	15	30	0.30	0.15
Soil Foundation	30	1600	20	10	0.35	0.2

In this paper, to realize the absorbing radiation wave, the viscous boundary [19] is adopted, and the formula, as shown in Formula (3.6), of normal viscous force and tangential

viscous force expressed by stress time history.

(3.6)
$$\begin{cases} C_P = \rho A \sqrt{\dfrac{\lambda + 2G}{\rho}} \\ C_S = \rho A \sqrt{\dfrac{G}{\rho}} \end{cases}$$

where A is the area of the section, C_P and C_S are normal parameters and tangential parameters respectively.

The onsite test section adopts a standard test vehicle with an axle load (single-axle double-wheel set) of 100 kN and a speed of 60 km/h, and the comparison result is shown in Fig. 4. According to Fig. 4, it can be seen that the dynamic stress data of the under-wheel area calculated by finite element method in this paper is consistent with the field measured values, with the maximum relative error of dynamic stress being 5.1%, and the sum of squared relative errors being 0.8%.
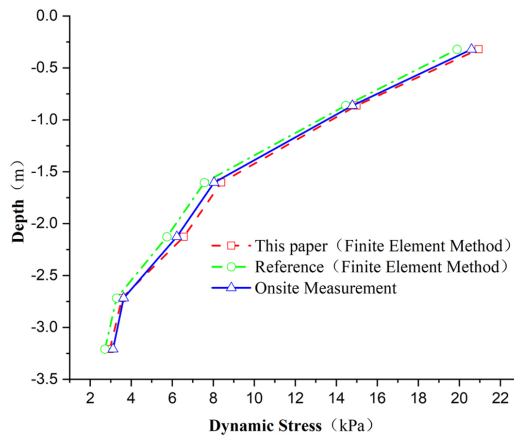
Fig. 4. Onsite model to Calculation model

4. Study on subgrade service depth

4.1. Definition of subgrade working area

The range where the dynamic stress generated by the moving vehicle load in the subgrade is greater than $\dfrac{1}{10}$ of the soil weight is called the subgrade working area [2, 4, 10] so there is Formula (4.1):

(4.1)
$$K = \frac{\sigma_z(x, y, z, t)}{\gamma_N \left(z - \sum\limits_{i=1}^{N-1} h_i\right) + \sum\limits_{i=1}^{N-1} \gamma_i h_i}$$

where σ_z is dynamic stress of subgrade, kN/m^2, N is ordinal number of current calculation layer, h_i is thickness of the i-th layer structure, m, γ_i is unit weight of the i-th layer structure, kN/m^2, K is ratio of vehicle load dynamic stress and soil weight.

4.2. Superposition characteristics of subgrade dynamic stress

The base course structure has diffusion effect on stress. The load of moving vehicle acts on the surface course and then is transmitted to the base course, which further diffuses the stress. When the dynamic stress distribution is intersected, the stress will be superimposed. Fig. 5 – (5a) front view, (5b) bottom view

| (a) Front view | (b) Bottom view |

Fig. 5. Peak dynamic stress iso-surface ($\delta_{zz} = -15$ kPa)

| (a) Front view | (b) Bottom view |
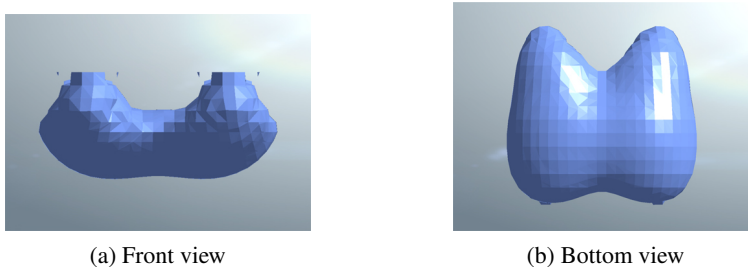
Fig. 6. Peak dynamic stress iso-surface ($\delta_{zz} = -10.5$ kPa)

Fig. 7 are isosurface distribution diagrams of peak stress under the action of 100 kN moving vehicle load. With the decrease of subgrade dynamic stress, the shape of dynamic stress isosurface changes from bimodal pattern to unimodal pattern.

Fig. 8 shows the variation of peak dynamic stress with depth under different axial loads. Fig. 8a is a graph showing the change of peak dynamic stress of the under-wheel grid unit with depth. The peak dynamic stress of under-wheel grid unit decays sharply with depth at first, and then converges gradually. Fig. 8b is a graph showing the change of peak dynamic stress of the centerline area grid unit with depth. In the area with small depth, the diffusion of dynamic stress is limited. The superposition effect of dynamic stress in the centerline area is not obvious, and its dynamic stress value is small. In the centerline area with deep

(a) Front view   (b) Bottom view

Fig. 7. Peak dynamic stress iso-surface ($\delta_{zz} = -6$ kPa)

depth, the dynamic stress distribution exists intersection, and because of the local symmetry of dynamic stress distribution, the dynamic stress on both sides forms vector superposition in the centerline area, which leads to the increase of dynamic stress value. With the further increase of the depth, the dynamic stress decays, and the distribution of dynamic stress in the centerline area increases at first and then decreases.

(a) Under-wheel   (b) Centerline
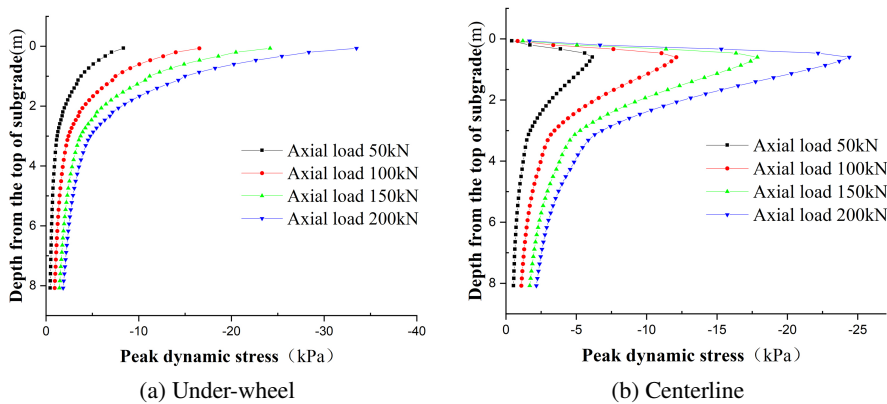
Fig. 8. Peak dynamic stress and depth

In the centerline area, the dynamic stress gradually increases to the peak point with the increase of depth, and the isosurface of dynamic stress completes the transformation from Fig. 5 to Fig. 6, when the superposition effect of dynamic stress induced by traffic load is the biggest. With the further increase of depth, the dynamic stress begins to decrease gradually, and the dynamic stress isosurface changes from Fig. 6 to (6a) Front view (6b) Bottom view

Fig. 7, and the dynamic stress isosurface changes from bimodal form to unimodal form. Thus, the depth required to transform the dynamic stress isosurface from bimodal form to unimodal form can be used as an index to describe the influence depth of stress superposition effect. Extracting the numerical simulation results, the influence depth of stress superposition effect can be obtained as (7a) Front view (7b) Bottom view

Fig. 7a. With the increase of axial load from 50 kN to 200 kN, the influence depth of superposition effect increases, which are 2.1 m, 2.6 m, 2.9 m and 3.2 m, and the growth rates are 19.2%, 10.3% and 9.4%, respectively.

4.3. Study on depth and influencing factors of subgrade working area

In the existing research, there is little analysis on the influence of superposition effect and dynamic action on subgrade service depth. Therefore, this section focuses on the difference of the depth of subgrade affected area between under-wheel area (stress superposition effect is not considered) and centerline area (stress superposition effect is considered) under dynamic and static axial load.

The ratio of the peak dynamic stress to the soil weight at the corresponding point is calculated by Formula (4.1). The change of the ratio of the dynamic stress to the soil weight with depth under the action of dynamic and static vehicle loads is shown in Figs. 9 and 10, where, Fig. (b) is an enlarged view for the red dotted frame in Fig. (a). In order to further obtain the accurate subgrade service depth, the right scatter diagram is fitted with the fitting formula as shown in Formula (4.2):

$$(4.2) \qquad\qquad K = a + be^{-kz}$$

where a, b and k are parameters to be determined, z is vertical distance from the calculation point to the top of the base course.

As shown in Fig. 9, when using dynamics to calculate, the ratio K of the under-wheel region attenuates exponentially with the increase of depth, while the ratio K of the midline region increases first and then decreases with the increase of depth. The subgrade service depth of each case can be calculated by fitting the calculated data. With the increase of axle load from 50 kN to 200 kN, the subgrade service depth under wheel increases, which is 1.60 m, 2.25 m, 2.67 m and 2.96 m, respectively. With the increase of axle load from


(a) Depth and ratio K (b) Enlarged map and fitting curves of dotted frame
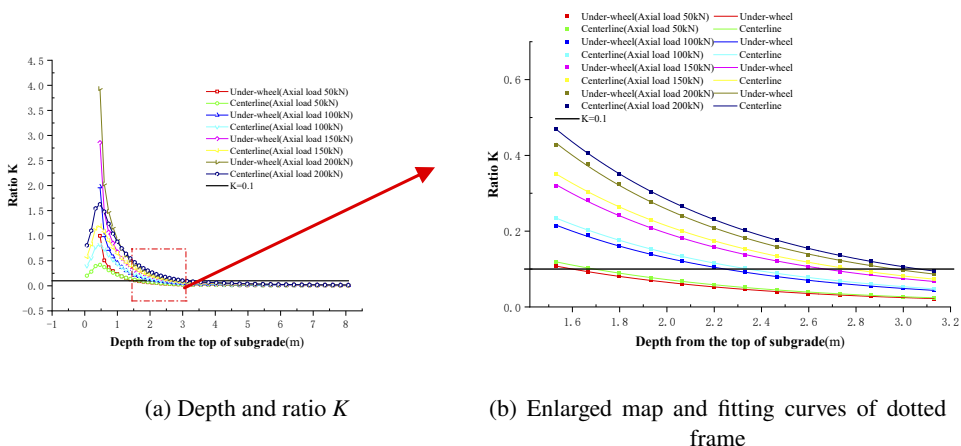
Fig. 9. Axle load to ratio K (Dynamics)

50 kN to 200 kN, the subgrade service depth in the centerline area increases, which is 1.69 m, 2.34 m, 2.78 m and 3.07 m, respectively.

As shown in Fig. 10, when the static method is used for calculation, no superposition effect of stress is observed in the centerline area. With the increase of depth, the ratio K in the under-wheel region and the centerline region shows exponential decay. With the increase of axle load from 50 kN to 200 kN, the subgrade service depth in the under-wheel region is 0.75 m, 1.29 m, 1.65 m and 1.94 m, respectively. With the increase of axle load from 50 kN to 200 kN, the subgrade service depth in the centerline area is 0.77 m, 1.37 m, 1.76 m and 2.05 m, respectively.

(a) Depth and ratio K

(b) Enlarged map and fitting curves of dotted frame
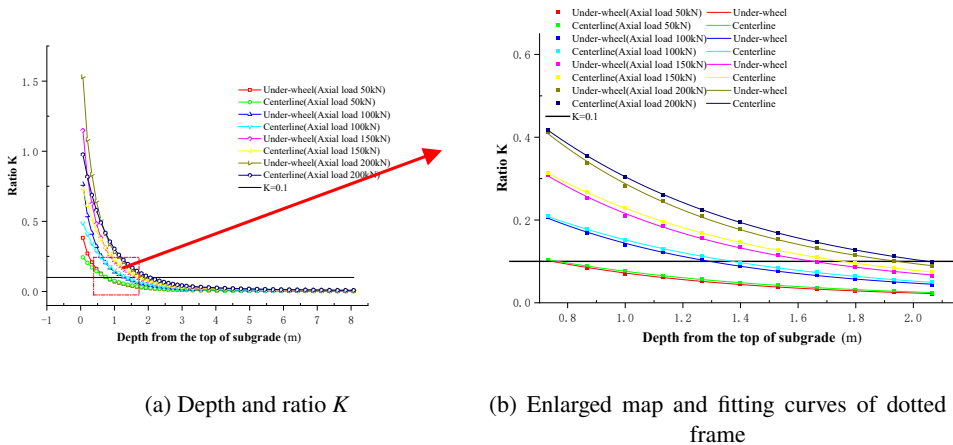
Fig. 10. Axle load to ratio K (Statics)

Levenberg–Marquardt optimization algorithm is used as the fitting method. All the determination coefficients R^2 are greater than 0.99. The fitting function can be used to calculate the subgrade service depth under various working conditions when $K = 0.1$, and the calculation results are shown in Fig. 11.

Considering the variation trend of peak dynamic stress increasing with depth, the variation trends of soil weight and scatter data in the under-wheel area and the centerline area, selecting negative power exponential function as the fitting function can better reflect the relationship between axle load and subgrade service depth. The fitting formula is the same as Formula (4.2), and Levenberg–Marquardt optimization algorithm is also adopted. The fitting goodness of the four fitting curves is good, and all the determination coefficients R^2 are greater than 0.999. The fitting formula of the four curves is shown in Formula (4.3):

$$(4.3) \quad \begin{cases} \text{Under-wheel(dynamic force)} : z = 3.54796 - 2.90345e^{-0.008P_z} \\ \text{Centerline(dynamic force)} : z = 3.64786 - 2.93023e^{-0.00809P_z} \\ \text{Under-wheel(static force)} : z = 2.61928 - 2.61681e^{-0.00673P_z} \\ \text{Centerline(static force)} : z = 2.64629 - 2.74502e^{-0.0076P_z} \\ 50 \text{ kN} \leq P_z \leq 200 \text{ kN} \end{cases}$$
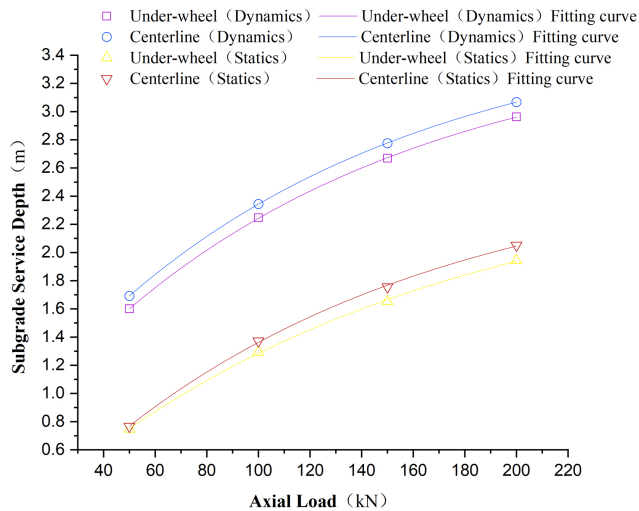
Fig. 11. Axle load and subgrade service depth

As shown in Fig. 11, axial load is an important factor affecting subgrade service depth. With the increase of axial load, the subgrade service depth will increase obviously, while the increasing rate of subgrade service depth will gradually decrease with the continuous increase of axial load. In addition, stress superposition effect is produced in the centerline area under the action of vehicle loads in both static and dynamic forms: In the range of 50 ~ 200 kN axle load, the function curve of subgrade service depth and axle load in the centerline area is completely above the function curve in the under-wheel area. Furthermore, with the increase of axle load, the function of the centerline area is further separated from the function of the under-wheel area, which means that increasing axle load will lead to the enhancement of superposition effect in the centerline area. It can be predicted that with the further increase of axle load, the subgrade service depth in the centerline area will remain greater than that in the under-wheel area.

The influence of wheel distance on subgrade service depth is shown in Fig. 12. With the increase of wheel distance, the stress superposition effect decreases. With the increase of wheel distance from 1.6 m to 2.5 m, the influence depth of stress superposition effect is 1.88 m, 1.58 m, 1.17 m and 0.62 m, respectively. With the increase of wheel distance from 1.6 m to 2.5 m, the subgrade service depth decreases, which is 2.58 m, 2.51 m, 2.46 m and 2.38 m, respectively.

As shown in Fig. 13, the influence of vehicle velocity on the subgrade service depth is significant. With the increase of vehicle velocity, the contact time between the wheel and the ground decreases, and the dynamic stress of the subgrade induced by the wheel decreases. With the increase of vehicle speed from 30 km/h to 150 km/h, the subgrade service depth decreases, which is 2.62 m, 2.53 m, 2.45 m and 2.38 m, respectively. With the increase of vehicle speed from 30 km/h to 150 km/h, the influence depth of stress superposition effect is 1.86 m, 1.82 m, 1.47 m and 1.15 m, respectively.

(a) Depth and ratio *K*

(b) Enlarged map and fitting curves of dotted frame
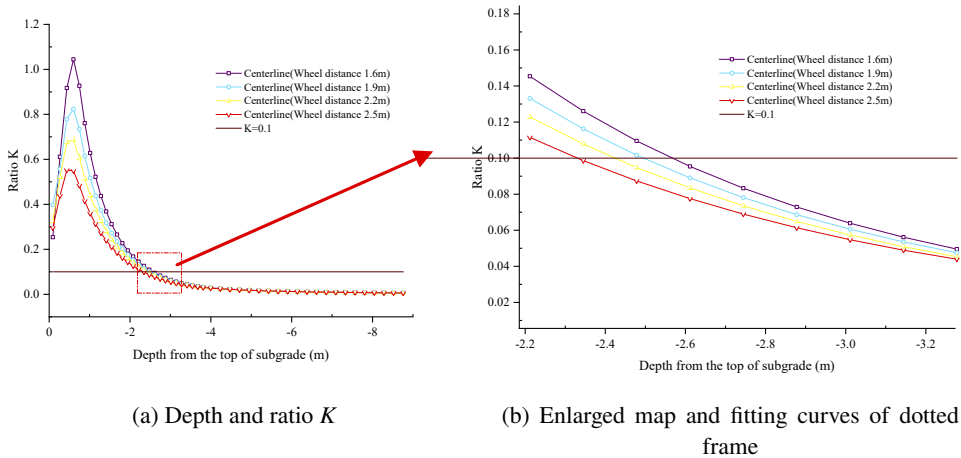
Fig. 12. Wheel distance to ratio *K*

(a) Depth and ratio *K*

(b) Enlarged map and fitting curves of dotted frame
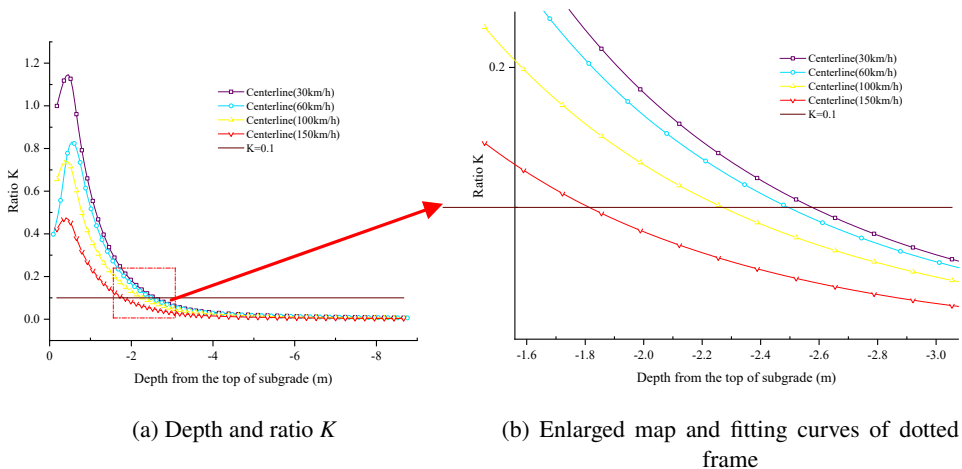
Fig. 13. Vehicle velocity to ratio *K*

5. Conclusions

1. On the basis of the establishment of the calculation model of composite elastic layer structure under moving vehicle load action, the analytical solution of dynamic mechanical response of moving vehicle load to composite elastic layer is obtained based on elastic mechanics and integral transform method.

2. Distribution characteristics of subgrade dynamic stress: the subgrade dynamic stress in the under-wheel area decays rapidly along the depth direction, while the subgrade dynamic stress in the centerline area between the two wheels increases first and then decreases along the depth direction. With the decrease of subgrade dynamic stress,

the shape of dynamic stress isosurface changes from bimodal pattern to unimodal pattern.

3. Under both static and dynamic axle loads, the subgrade service depth in the centerline area is always greater than that in the under-wheel area. Under the action of the same axle load, the subgrade service depth calculated by dynamic action is less than that by dynamic action. Obviously, the subgrade service depth calculated by considering both stress superposition effect and dynamic action is safer and more reasonable.

4. The wheel distance and vehicle velocity have a significant influence on the subgrade service depth.With the increase of wheel distance from 1.6 m to 2.5 m, the subgrade service depth decreases, which is 2.58 m, 2.51 m, 2.46 m and 2.38 m, respectively. With the increase of vehicle speed from 30 km/h to 150 km/h, the influence depth of stress superposition effect is 1.86 m, 1.82 m, 1.47 m and 1.15 m, respectively.

References

[1] Wang Chang-Jing, *Study on the dynamic stress in ground induced by train moving load and cyclic properties of soft saturated clay*. Zhejiang University, 2006.

[2] Liu Da-Peng, *Study on the Engineering Properties of Aeolian Sand and Gravel Soil Low Embankment Under Vehicle Load*. Chang'an University, 2015.

[3] Y. Momoya, E. Sekine, F. Tatsuoka, "Deformation characteristics of railway roadbed and subgrade under moving-wheel load", *Soils and Foundations*, 2005, vol. 45, no. 4, pp. 99–118, DOI: 10.3208/sandf.45.4_99.

[4] Lu Zheng, Wang Chang-Bo, Fu Jian-Jun, et al., "Research on influence depth of road subgrade induced by vehicle loads", *Rock and Soil Mechanics*, 2013, vol. 34, no. 02, pp. 316–321+352, DOI: 10.16285/j.rsm.2013.02.030.

[5] X. Ma, *Analytical solutions and monitoring methodology for mechanical responses of asphalt pavement subjected to random loads*. Harbin Institute of Technology, 2019.

[6] Z. Dong, X. Ma, "Analytical solutions of asphalt pavement responses under moving loads with arbitrary non-uniform tire contact pressure and irregular tire imprint", *Road Materials & Pavement Design*, 2017, vol. 19, no. 8, pp. 1–17, DOI: 10.1080/14680629.2017.1354776.

[7] W. Liu, H. Mei, W. Leng, et al., "Numerical Analysis of Dynamic Stress Response Characteristics of Subgrade Bed", *Journal of the China Railway Society*, 2017, vol. 39, no. 12, pp. 108–117, DOI: 10.3969/j.issn.1001-8360.2017.12.015.

[8] F. Xu, Q. Yang, W. Leng, et al., "Dynamic Stress of Subgrade Bed Layers Subjected to Train Vehicles with Large Axle Loads", *Shock and Vibration*, 2018, vol. 2018, pp. 1–12, DOI: 10.1155/2018/2916096.

[9] M. Liu, W. Peng, Y. Gao, "Analytical solution of the dynamic stress of elastic multi-layered medium under moving strip load", *China Civil Engineering Journal*, 2010, vol. 43, no. 3, pp. 81–87, DOI: 10.15951/j.tmgcxb.2010.03.002.

[10] Z. Yang, G. Cheng, "Quantitative analysis of influencing factors of subgrade service depth of civil airport runway", *Chinese Journal of Geotechnical Engineering*, 2016, vol. 38, pp. 130–135, DOI: 10.11779/CJGE2016S2021.

[11] C. Qu, K. Kang, L. Wei, et al., "Research on dynamic response characteristics and long-term dynamic stability of subgrade-culvert transition zone in high-speed railway", *Rock and Soil Mechanics*, 2020, vol. 41, no. 10, pp. 1–11, DOI: 10.16285/j.rsm.2020.0079.

[12] Y. Shang, L. Xu, Y. Cai, "Study on Dynamic Features of Cement-Stabilized Expansive Soil Subgrade of Heavy Haul Railway under Soaking Environment", *Rock and Soil Mechanics*, 2020, vol. 41, no. 8, pp. 1–8, DOI: 10.16285/j.rsm.2019.1467.

[13] K. Wang, Y. Zhuang, X. Gen, "Experimental study on critical dynamic stress of coarse-grained soil in railway subgrade", *Rock and Soil Mechanics*, 2020, vol. 41, no. 6, pp. 1865–1873, DOI: 10.16285/j.rsm.2019.1511.

[14] X. Yang, Q. Wan, D. Liu, et al., "Dynamic characteristics of gravel soil low embankment in Xinjiang", *Journal of Traffic and Transportation Engineering*, 2019, vol. 19, no. 3, pp. 1–9, DOI: 10.19818/j.cnki.1671-1637.2019.03.001.

[15] Y. Zhao, Z. Wang, G. Wang, et al., "Stress pulse durations in asphalt pavement under moving load", *Journal of Traffic and Transportation Engineering*, 2009, vol. 9, no. 6, pp. 11-15, DOI: 10.19818/j.cnki.1671-1637.2009.06.003.

[16] Z. Lu, H. Yao, W. Wu, et al., "Structural analysis and design method of dynamic deformation of expressway subgrade", *Rock and Soil Mechanics*, 2010, vol. 31, no. 9; pp. 2907–2912, DOI: 10.16285/j.rsm.2010.09.013.

[17] L. An, F. Zhang, Y. Geng, et al., "Field Measurement of Dynamic Compressive Stress Response of Pavement-Subgrade Induced by Moving Heavy-Duty Trucks", *Shock and Vibration*, 2018, vol. 2018, pp. 1–12, DOI: 10.1155/2018/1956906.

[18] G. Liao, X. Huang, *Application of ABAQUS finite element Software in Road Engineering*. Southeast University Press, 2008.

[19] H. Fu, J. Liu, L. Zhang, et al., "Dynamic stability analysis for rock slope based on orthogonal test", *Journal of Central South University (Science and Technology)*, 2011, vol. 42, no. 9, pp. 2853–2859.